International Journal of Geo-Information

MDPI

Article

Regional Terrain Complexity Assessment Based on Principal Component Analysis and Geographic Information System: A Case of Jiangxi Province, China

Faming Huang [1], Jianbo Yang [1], Biao Zhang [1], Yijing Li [1,*], Jinsong Huang [2] and Na Chen [3]

[1] School of Civil Engineering and Architecture, Nanchang University, Nanchang 330031, China; faminghuang@ncu.edu.cn (F.H.); jiawu_chen@email.ncu.edu.cn (J.Y.); 416114417186@email.ncu.edu.cn (B.Z.)
[2] ARC Centre of Excellence for Geotechnical Science and Engineering, University of Newcastle, Newcastle, NSW 2308, Australia; jinsong.huang@newcastle.edu.au
[3] School of Civil Engineering and Architecture, Hubei University of Technology, Wuhan 430068, China; cn_research@hbut.edu.cn
* Correspondence: ejinn@ncu.edu.cn

Received: 13 August 2020; Accepted: 7 September 2020; Published: 8 September 2020

Abstract: Regional terrain complexity assessment (TCA) is an important theoretical foundation for geological feature identification, hydrological information extraction and land resources utilization. However, the previous TCA models have many disadvantages; for example, comprehensive consideration and redundancy information analysis of terrain factors is lacking, and the terrain complexity index is difficult to quantify. To overcome these drawbacks, a TCA model based on principal component analysis (PCA) and a geographic information system (GIS) is proposed. Taking Jiangxi province of China as an example, firstly, ten terrain factors are extracted using a digital elevation model (DEM) in GIS software. Secondly, PCA is used to analyze the information redundancy of these terrain factors and deal with data compression. Then, the comprehensive evaluation of the compressed terrain factors is conducted to obtain quantitative terrain complexity indexes and a terrain complexity map (TCM). Finally, the TCM produced by the PCA method is compared with those produced by the slope-only, the variation coefficient and K-means clustering models based on the topographic map drawn by the Bureau of Land and Resources of Jiangxi province. Meanwhile, the TCM is also verified by the actual three-dimensional aerial images. Results show that the correlation coefficients between the TCMs produced by the PCA, slope-only, variable coefficient and K-means clustering models and the local topographic map are 0.894, 0.763, 0.816 and 0.788, respectively. It is concluded that the TCM of the PCA method matches well with the actual field terrain features, and the PCA method can reflect the regional terrain complexity characteristics more comprehensively and accurately when compared to the other three methods.

Keywords: terrain complexity assessment; digital elevation model; principal component analysis; variation coefficient method; K-means clustering; geographic information system

1. Introduction

Regional terrain complexity assessment (TCA) is a meaningful foundation for identifying regional geological features, estimating groundwater level and river information and effectively utilizing the land resources in order to promote social and economic development [1–4]. Hence, it is significant to strengthen the TCA research and produce terrain complexity maps (TCM) in the areas with mountainous and hilly landforms [5–7].

The modeling of TCA includes multiple processes, such as acquisition of data sources, assessment unit division, selection of terrain factors and assessment model building. Recently, the technologies of remote sensing (RS) and geographic information systems (GIS) provide accurate and abundant data for regional TCA; therefore, the terrain factors used in this study are also acquired based on RS and GIS [8–11]. Furthermore, it is very important to select an appropriate model for TCA. In response to this issue, some scholars have proposed a lot of TCA-related models in recent years. Some of these models describe the regional terrain complexity only using a single terrain factor; for example, Tianwen, et al. [12] and Huaxing, et al. [13] selected slope angle as the terrain factor of TCA; Long et al. [14] used the fractal dimension value to describe the terrain complexity; Ashenfelter and Eberhard [15] adopted the angle between the space planes to describe the terrain complexity. These studies are unable to comprehensively reflect the terrain features of the study areas because they select limited terrain factors for TCA. On the other hand, some scholars used several types of terrain factors to determine the regional terrain features. For example, Chambers, et al. [16] pointed out that the regional differentiation laws of terrain complexity can be reflected by the synthesis calculations of terrain factors; Huaxing, Liu and Tang [13] explored the composite terrain factors based on a digital elevation model (DEM) to reflect the change characteristics of topographic relief and folds respectively from the holistic and local perspectives; Rawat and Joshi [17] studied the regional terrain characteristics in the land suitability classification; Thompson, et al. [18] analyzed the effects of DEM with different spatial resolutions on TCA and land landscape simulation.

In any case, there are still several problems in the previous models (variation coefficient method, k-means clustering method, etc.) which need to be solved, such as the need to introduce more terrain factors to TCA models, the lack of consideration of redundant information between terrain factors and the quantitative computation of the terrain complexity indexes. That is to say, the previous method cannot deal with the redundant information between the ten terrain factors. As a result, the TCA accuracy may be reduced. Furthermore, it is difficult for the previous methods to calculate the terrain complexity indexes quantitatively. Therefore, it is necessary and significant to propose a novel model which is appropriate for quantitatively and accurately analyzing a lot of terrain factors and can solve multifactor collinearity problems.

In this study, an excellent and widely acknowledged multivariate statistical method, namely principal component analysis (PCA), is proposed to work with TCA to overcome the drawbacks of the previous models. The PCA method can effectively calculate the component scores from the extracted principal components. Generally, the calculated component scores can be considered as the quantitative terrain complexity indexes, which are helpful to introduce regional topographic features into engineering applications. Then, the comprehensive assessment results can be accurately calculated by the PCA method [19]. The PCA model has been successfully used in various research fields [20–23]. For example, Li et al. [24] proposed the PCA and high-dimensional model representation techniques to estimate the probabilistic power flow; Geng, et al. [25] used the PCA based long short-term memory network to predict short-term wind speed time series; Schwartz, et al. [26] proposed a robust PCA method to conduct change detection in ultrawideband synthetic aperture radar images; Gao, et al. [27] researched network intrusion detection using extreme learning machine and adaptive PCA methods. However, the PCA method has received little attention in the field of regional TCA. Therefore, the PCA method is used to deal with the terrain factor compression and quantitative calculation of TCA.

The Jiangxi province of China is taken as the research area because the terrain of Jiangxi province is very complex, with types of high mountains and hills and so on. Moreover, complex terrain environments limit the local geological survey and land use planning. Hence, this paper firstly extracts several terrain factors using the DEM data in the GIS software and proposes the PCA method to calculate the terrain complexity indexes of Jiangxi province. Then, the influences of the extracted terrain factors on terrain complexity are explored. Moreover, the TCA results of PCA are compared with those of the slope-only method (considering only the slope map as the TCA map), variation coefficient method and k-means clustering model to discuss the modeling performance of PCA.

2. Materials and Methods

2.1. Introduction of Jiangxi Province and Data Sources

Jiangxi province is located in Eastern China, between 24°29′14″ *N*~30°04′41″ *N* and 113°34′36″ *E*~118°28′58″ *E*, with a length of 620 km from north to south and 490 km from east to west, covering an area of 166,900 km^2 (Figure 1). Jiangxi province is mainly hilly and mountainous, with extensive basins and valleys. This province is relatively flat in the northern part, surrounded by mountains on three sides in the eastern, western and southern parts, and is hilly in the middle part, making it a huge basin inclined toward Poyang Lake and opening to the north. The Ganjiang river, Fuhe river, Xinjiang river, Xiuhe river and Raohe river are the five major rivers that flow through Jiangxi province, and Poyang Lake is the largest freshwater lake in China. This province has a subtropical humid climate, with annual average rainfall ranging from 1341 to 1940 mm.

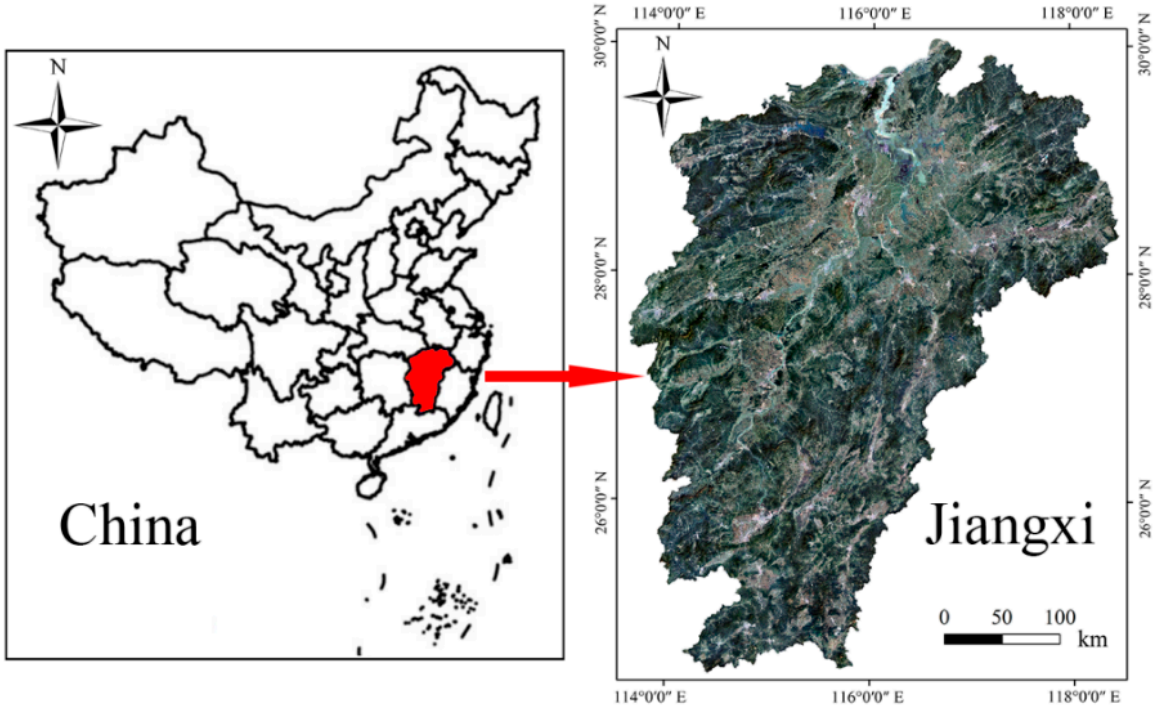

Figure 1. Aerial images of Jiangxi province.

2.2. Description of Terrain Factors

The data sources used for TCA modeling include (1) the topography data acquired through field survey; (2) the aerial images taken by the unmanned aerial vehicle on 1st February 2018 (freely downloaded from Google Earth 7.1.8.3036 (32-bit) with spatial resolution of 1.09 m); (3) DEM data with 100 m resolution taken on 11th February 2000 for extracting terrain factors (freely downloaded from http://www.gscloud.cn/) [28,29]; (4) the local topographic map with 1:250,000 scale. The Jiangxi province is divided into 16,713,615 grid cells with 100 m grid resolution—this is because this resolution can effectively characterize the topographical features of the study area, and it will not lead to too much computation as a result of mass grid cells [30].

In this study, ten terrain factors (including elevation (m), slope (°), plan curvature, profile curvature, relief amplitude (m), surface roughness, surface cutting depth (m), gully density (m/m^2), elevation variation coefficient and slope length (m)) from the above data sources are extracted by the spatial analysis function of ArcGIS 10.2 software. All the ten terrain factors are respectively divided into five classes using the natural breakpoint method [31–33]. This is because the natural breakpoint method can effectively identify the frequency distribution characteristics of terrain factors to obtain the best

class division scheme, and it has been successfully used in the research of the class divisions by many other scholars [34–37]. The purpose of class division is to better represent the distribution rules of these terrain factors (Figure 2). In fact, the standardized results of terrain factors are the final input variables of all the TCA models.

(1) Elevation

The elevation [36,38] of the study area ranges from 2 to 2147 m. The mountains with high elevation mainly distribute around the Jiangxi province, while the central area of Jiangxi province has relatively low elevation. Generally speaking, the higher the elevation in the southern hilly area, the greater the terrain complexity (Figure 2a).

(2) Slope

According to the slope classification standard and the actual slope characteristics, the slopes of the study area are divided into five classes as flat slope, gentle slope, moderate slope, steep slope and acute slope [39–42]. The area with gentle slope covers around 33.88% of the total study area. The greater the slope, the more complex the terrain. To produce TCM based on the slope-only model, the flat slope, gentle slope, moderate slope, steep slope and acute slope in Jiangxi province are respectively considered as very low, low, moderate, high and very high complex terrain levels.

(3) Plan curvature and profile curvature

Plan curvature and profile curvature respectively reflect the change characteristics of concave and convex terrains from the horizontal direction and vertical direction [43]. The plan curvature (Figure 2b) can be determined by calculating the slope aspect of a slope map. Meanwhile, the profile curvature (Figure 2c) can be determined by calculating the slope twice on the basis of the DEM map [44]. In general, the greater the profile curvature or plan curvature, the higher the terrain complexity. However, compared with profile curvature, plan curvature has less correlation with terrain complexity.

(4) Relief amplitude

The relief amplitude of the study area can be obtained through the statistical test and the maximum height difference method. The greater the relief amplitude, the higher the terrain complexity [45]. According to Liu [46], the study area can be divided into five grades: plain region, tableland, hill, small rolling mountain and mountain. The results in Figure 2d show that the main terrain relief types of Jiangxi province are hill and small rolling mountain.

(5) Surface cutting depth

Surface cutting depth is defined as the difference between average elevation and minimum elevation in a certain area of one point on the ground surface [47]. In this study, the calculation radius of surface cutting depth is set to be 12 grid cells and the calculation results are shown in Figure 2e. Generally, a greater surface cutting depth means higher terrain complexity [48].

(6) Surface roughness

The surface roughness, which is an important index reflecting surface relief and soil erosion degree, is defined as the ratio of surface area to its projected area in a certain grid cell (Figure 2f). The surface roughness can be determined using the grid calculator of ArcGIS software according to Equation (1), where *Rou* is the surface roughness value, and *S* is the slope value of the study area. The greater the surface roughness, the higher the terrain complexity [49].

$$Rou = 1/\mathrm{Cos}(S * 3.14159/180) \quad (1)$$

(7) Gully density

The gully density (Figure 2g) is defined as the total length of the river network in a unit area [50,51]. The river network in a study area can be extracted by the hydrological analysis tool of ArcGIS 10.2 software. Then, we can calculate the gully density through the grid calculator, as shown in Equation (2), where D_S is the gully density, and L is length of the river networks in a unit area A.

$$D_S = \sum L/A \quad (2)$$

(8) Elevation variation coefficient

Elevation variation coefficient (Figure 2h) can be expressed as the ratio of the standard deviation of elevations to their average value in a certain area. This terrain factor is in direct proportion to the terrain complexity [52,53].

(9) Slope length

Slope length (Figure 2i) suggests the projected length of the maximum ground distance on a horizontal plane, from a point on the ground to its starting point in the direction of water flow [54,55]. Slope length affects terrain complexity indirectly and its formula is expressed in Equation (3), where m indicates the flow length on the ground surface in the direction of water flow, and S is the slope value of the ground surface.

$$L = m \times \cos(S) \tag{3}$$

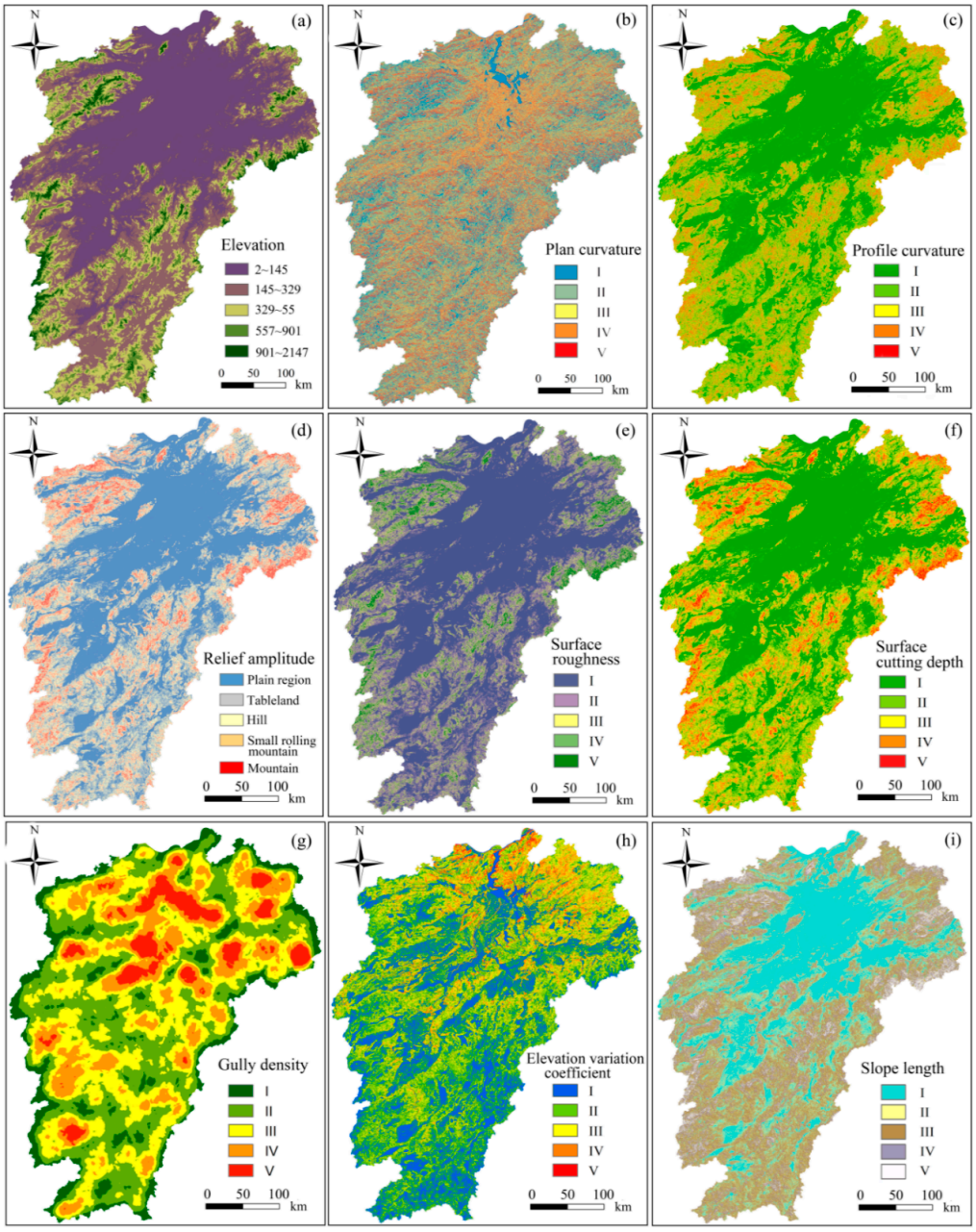

Figure 2. Terrain factors: elevation (**a**), plan curvature (**b**), profile curvature (**c**), relief amplitude (**d**), surface roughness (**e**), surface cutting depth (**f**), gully density (**g**), elevation variation coefficient (**h**), slope length (**i**).

2.3. Modeling Procedures of TCA

The modeling procedures of TCA using the PCA method are shown in Figure 3:

(1) All ten types of terrain factors are extracted and graded from the DEM data using spatial analysis tools and data management tools in ArcGIS 10.2 software.

(2) The PCA method is used to conduct quantitative calculation of topographic complexity indexes based on the covariance matrix of the above terrain factors. The principal components with cumulative contribution rates greater than 90% are adopted to calculate the component scores, which are considered the terrain complexity indexes.

(3) The slope-only, variation coefficient and k-means clustering methods are respectively used to assess the topographic complexity for comparisons. Their TCA results are also classified into five levels, namely very low, low, moderate, high and very high terrain complexity.

(4) The TCMs of Jiangxi province are produced in ArcGIS 10.2 by the above four methods.

(5) The accuracy of these TCMs is evaluated using the correlation coefficients between the TCMs and the topographic map and also evaluated through matching with the actual three-dimensional aerial images.

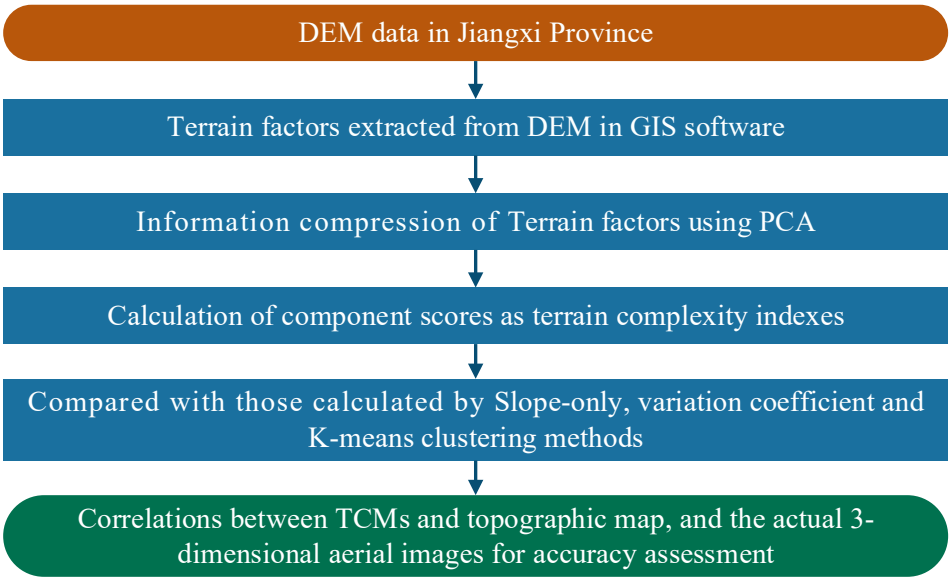

Figure 3. Flow chart of principal component analysis method for terrain complexity assessment.

2.4. Description of the Methods

2.4.1. Principal Component Analysis

The PCA method aims to use the idea of dimensionality reduction to transform multiple factors into a few principal components. Each principal component can reflect a piece of information of the original variables [56]. Furthermore, the contained information of each principal component is not repeated with that of other principal components. The PCA converts a given set of related variables into another set of unrelated variables through a linear transformation. Then, these new uncorrelated variables are arranged in descending order of variance. Initially, when using the PCA method, the dimensionality of all terrain factors should be unified. Supposing the original data set $x_{ij}, i = 1, 2, \cdots\cdots, n;\ j = 1, 2, \cdots\cdots m$ is composed by n grid cells with m types of terrain factors, the data set x_{ij} can be standardized by column as

$$x_{ij}^{*} = \frac{x_{ij} - \overline{x}_j}{\sigma_j},\ i = 1, 2, \cdots\cdots, n,\ j = 1, 2, \cdots\cdots, m \tag{4}$$

$$\sigma_j = \sqrt{\frac{1}{n-1}\sum_{i=1}^{n}\left(x_{ij} - \overline{x}_j\right)^2} \tag{5}$$

where x_{ij}^* is the standardized result of x_{ij}, $\overline{x}_j$ is the mean value of x_j, and σ_j is the standard deviation of x_j. The correlation coefficient matrix of x_{ij}^* is first calculated. Then, the eigenvalues λ and their corresponding eigenvectors are calculated based on the correlation coefficient matrix. The contribution rate of each eigenvalue can be obtained using Equation (6), where k is the number of eigenvalues.

$$V_i = \frac{\lambda_i}{\sum_{i=1}^{k}\lambda_i} \tag{6}$$

According to the eigenvalue and its eigenvector, the physical significance of the principal components is explained. According to the load coefficient value of the selected principal component in each terrain factor, the weight coefficient value of each terrain factor in the selected principal component is calculated by the following formula:

$$a_{ij} = l_{ij}/\sqrt{\lambda_i} \tag{7}$$

where a_{ij} and l_{ij} are respectively the weight coefficient value and load coefficient value of the j-th terrain factor in the i-th principal component; λ_i is the eigenvalue corresponding to the i-th principal component. Then, the comprehensive factor of each principal component can be calculated as

$$F_i = \sum\nolimits_{j=1}^{m} a_{ij} \times x_j \tag{8}$$

where F_i is the comprehensive factor of all the terrain factors, and m is the number of terrain factors. Finally, the comprehensive scores of the selected principal components are obtained by Equation (9), where V is the total contribution rate of the selected principal components; T is the number of retained principal components; V_i is the contribution rate of the i-th principal component.

$$F = \sum\nolimits_{i=1}^{T} \frac{V_i}{V} \times F_i \tag{9}$$

2.4.2. Variation Coefficient Method

The variation coefficient, which is an objective weighting method, directly uses the information contained in each factor to calculate the weight of the factor [57,58]. The basic idea of this method is that, in the evaluation factor system, the greater the difference of the values contained in a factor, the more the influence of a factor on the evaluated object. The differences between the values contained in a factor can be measured using the variation coefficient of this factor as

$$VC_j = \frac{\sigma_j}{\overline{x}_j}, j = 1, 2, 3, \ldots\ldots m \tag{10}$$

where VC_j is the variation coefficient of the j-th factor, also known as the standard deviation coefficient; σ_j and $\overline{x}_j$ are respectively the standard deviation and mean values of the j-th factor. Then, the weight of each factor is calculated as

$$W_j = \frac{VC_j}{\sum_{j=1}^{m} VC_j} \tag{11}$$

2.4.3. K-Means Clustering Model

The K-means clustering model [59,60] firstly sets the number of clusters K and the initial center point of each cluster and then updates the center point and optimizes the clustering results in an iterative way. The specific steps are as follows:

(1) We set a training sample $S = \{x_1, x_2, \cdots, x_m\}$, where $x_m \in R^n$ and m represents the number of samples. K clusters of $(SD_1, SD_2, \cdots, SD_K)$ are set as the output. Meanwhile, K clustering center points are selected and denoted as $u_1, u_2, \cdots, u_k$.

(2) Empty K clusters in turn as $SD_j = \{\}$, $j = 1, 2, \cdots, k$. For each sample x_p in the training set S, its distance to the K center points is respectively calculated, and then it is classified into the corresponding cluster with the smallest distance to the center point of the cluster. In Equations (12) and (13), C_p denotes the cluster which x_p belongs to

$$C_p = \underset{j}{\operatorname{argmin}} \|x_p - u_j\| \tag{12}$$

$$SD_{C_p} = \left\{SD_{C_p}, x_p\right\} \tag{13}$$

(3) For each cluster SD_i, its center point μ_i is recalculated according to Equations (14) and (15), where the $sum\_feature\ (SD_i)$ is the sum of the characteristic values of all samples in cluster SD_i, and the $sum\_number(SD_i)$ is the number of samples in cluster SD_i.

$$\mu_i = \frac{sum\_feature(SD_i)}{sum\_number(SD_i)} = \frac{\sum_{p=1}^{m} x_p SD_{i,p}}{\sum_{p=1}^{m} SD_{i,p}} \tag{14}$$

$$SD_{i,p} = \begin{cases} 1, C_p = i \\ 0, C_p \neq i \end{cases} \tag{15}$$

(4) Repeat steps 2 and 3 until the cost function is less than the given threshold. Equation (16) is set as the cost function, which denotes the sum of Euclidean distances between all samples in the sample set S and the center points of their corresponding clusters.

$$J(u, c) = \sum_{p=1}^{m} \|x_p - u_{C_p}\|^2 \tag{16}$$

3. Results

3.1. TCA Using Principal Component Analysis

3.1.1. Terrain Factor Analysis

The selected terrain factors are standardized, and then the Kaiser-Meyer-Olkin (KMO) test and Bartlett spherical test of the PCA method are performed based on the standardized data. Results show that the KMO test value of the standardized data is 0.790 (greater than 0.6) and its Bartlett spherical test value is less than 0.05, indicating that the PCA method is appropriate for dealing with the selected terrain factors. The PCA method is conducted on all the grid cells in Jiangxi province through the covariance matrix of the selected terrain factors. Then, the eigenvalues and explanatory contribution rates of all principal components are obtained, as shown in Table 1.

Table 1. Eigenvalues and explanatory contribution rates of all principal components.

Principal Component	Eigenvalue	Explanatory Contribution Rate (%)	Cumulative Contribution Rate (%)
1	5.518	55.179	55.179
2	1.184	11.843	67.022
3	1.007	10.072	77.094
4	0.900	9.000	86.094
5	0.569	5.687	91.781
6	0.373	3.735	95.515
7	0.260	2.605	98.120
8	0.145	1.449	99.569
9	0.024	0.235	99.804
10	0.020	0.196	100

According to the results in Table 1, the principal components that can be used to describe the terrain factors are selected. Relevant studies suggest that the main information contained in primitive variables can be effectively interpreted by the corresponding principal components when their cumulative contribution rate reaches 90% [61]. It can be seen from Table 1 that the explanatory cumulative contribution rate of the first five principal components $F_{i1} \sim F_{i5}$ can reach 91.78%. Therefore, the $F_{i1} \sim F_{i5}$ (Table 2) are used to describe the terrain characteristics of Jiangxi province.

Table 2. Component matrix of the ten terrain factors.

Terrain Factors	F_{i1}	F_{i2}	F_{i3}	F_{i4}	F_{i5}
elevation (*E*)	0.780	−0.477	0.019	0.180	0.036
slope (*S*)	0.961	0.036	−0.085	0.066	−0.091
plan curvature (*Plc*)	−0.238	−0.107	0.927	0.198	−0.140
profile curvature (*Prc*)	0.724	0.044	0.251	−0.019	0.534
relief amplitude (*Rel*)	0.956	0.059	0.068	0.062	−0.130
surface roughness (*Rou*)	0.944	0.021	0.063	0.090	−0.147
surface cutting depth (*Scd*)	0.859	0.014	−0.131	0.159	−0.317
gully density (*Gd*)	−0.272	0.477	−0.127	0.812	0.134
elevation variation coefficient (*Evc*)	0.316	0.840	0.187	−0.335	−0.103
slope length (*L*)	0.829	0.067	0.001	−0.118	0.294

It can be seen from Tables 1 and 2 that the explanatory contribution rate of F_{i1} is 55.179%, and the maximum load in F_{i1} is *S*, with a load coefficient of 0.96, followed by the *Rel* and *Rou*, with load coefficients of 0.956 and 0.944, respectively. Therefore, F_{i1} is mainly used to describe the slope and relief amplitude of the study area. The explanatory contribution rate of F_{i2} is 11.843%, *Ecv* is the maximum load in F_{i2}, with a load coefficient of 0.840, and *Gd* is the second maximum load in F_{i2}, with a load coefficient of 0.477, indicating that F_{i2} is mainly used to describe the elevation variation coefficient and gully density of the study area. In addition, the explanatory contribution of F_{i3} is 10.072% and the maximum load in F_{i3} is *Plc*, with a load coefficient of 0.927, which suggests that F_{i3} is mainly used to describe the plan curvature. Based on Equation (8), the comprehensive factors of the selected five principal components F_{i1}~F_{i5} are calculated as follows:

$$\begin{aligned} F_{i1} = \; & 0.332 \times E + 0.409 \times S - 0.101 \times Plc + 0.308 \times Prc + 0.407 \times Rel + 0.366 \times Rou \\ & + 0.402 \times Scd - 0.116 \times Gd + 0.134 \times Ecv + 0.353 \times L \end{aligned} \tag{17}$$

$$\begin{aligned} F_{i2} = \; & -0.438 \times E + 0.033 \times S - 0.099 \times Plc + 0.041 \times Prc + 0.055 \times Rel - 0.012 \times Rou \\ & + 0.020 \times Scd + 0.438 \times Gd + 0.772 \times Ecv + 0.062 \times L \end{aligned} \tag{18}$$

$$\begin{aligned} F_{i3} = \; & 0.018 \times E - 0.084 \times S + 0.924 \times Plc + 0.250 \times Prc + 0.068 \times Rel - 0.131 \times Rou \\ & + 0.063 \times Scd - 0.126 \times Gd + 0.186 \times Ecv + 0.001 \times L \end{aligned} \tag{19}$$

$$F_{i4} = \begin{array}{l} 0.190 \times E + 0.070 \times S + 0.209 \times Plc - 0.020 \times Prc + 0.066 \times Rel + 0.168 \times Rou \\ +0.094 \times Scd + 0.856 \times Gd - 0.354 \times Ecv - 0.124 \times L \end{array} \quad (20)$$

$$F_{i5} = \begin{array}{l} 0.048 \times E - 0.120 \times S - 0.186 \times Plc + 0.708 \times Prc - 0.173 \times Rel - 0.421 \times Rou \\ -0.195 \times Scd + 0.178 \times Gd - 0.1377 \times Ecv + 0.390 \times L \end{array} \quad (21)$$

3.1.2. Terrain Complexity Assessment

According to Equation (9) and the five principal components $F_{i1} \sim F_{i5}$, the terrain complexity index F of each grid cell in Jiangxi province can be calculated as

$$F_i = 0.601 \times F_{i1} + 0.129 \times F_{i2} + 0.110 \times F_{i3} + 0.098 \times F_{i4} + 0.062 \times F_{i5} \quad (22)$$

The TCA results of Jiangxi province using the PCA method are shown in Figure 4a. The areas with very high and high terrain complexity levels are mainly distributed in the surrounding areas of Jiangxi province with continuous mountain ranges, accounting for 1.5% and 6.0% of the total area, respectively. These very high and high terrain complexity indexes are mainly affected by the great values of slope, elevation, relief amplitude, surface cutting depth, surface roughness and profile curvature. On the contrary, the very low and low complexity regions account for the largest area (36.6% and 40.7%, respectively) and are mainly distributed in central parts of Jiangxi province with small values of slope, elevation, relief amplitude, profile curvature and gully density. Furthermore, the moderate terrain complex areas account for 15.1% of the total area and are evenly distributed in the study area. The terrain complexity of Jiangxi province is at a low and middle level on the whole. The overall terrain complexity of the study area is in line with its topographic and geomorphic characteristics, which can be mainly described as middle and low mountains supplemented by hilly areas. Meanwhile, the TCA produced by the slope-only method is shown in Figure 4b for comparison, suggesting that the overall distribution rule of both TCMs is consistent.

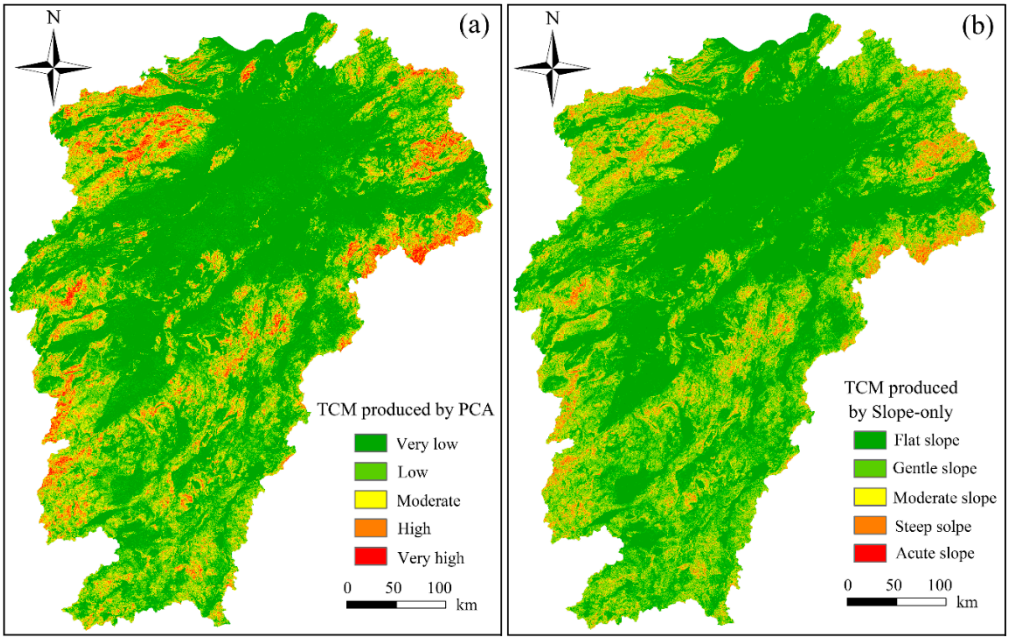

Figure 4. TCMs produced by the PCA (**a**) and slope-only (**b**) methods.

3.2. TCA Using Variation Coefficient Method

According to the selected terrain factors, the variable coefficient of each terrain factor is determined. In addition, the weight values of all terrain factors are calculated based on their variable coefficients, as shown in Table 3. Then, these weight values are put into Equation (11) to calculate the terrain

complexity indexes of Jiangxi province. The produced TCA results are shown in Figure 5a. It can be seen from Table 5 that the very low, low, moderate, high and very high terrain complexity areas account for around 36.64%, 40.72%, 15.14%, 6.04% and 1.46% of the total area, respectively.

Table 3. Variation coefficients and weight values of terrain factors.

Terrain Factor	*E*	*S*	*Plc*	*Prc*	*Rel*	*Rou*	*Scd*	*Gd*	*Ecv*	*L*
Variable coefficient	0.923	0.967	0.680	0.981	0.920	0.964	0.030	0.577	0.701	0.232
Weight value	0.132	0.139	0.097	0.141	0.132	0.138	0.004	0.083	0.101	0.033

3.3. TCA Using K-Means Clustering Model

The selected standardized terrain factors are put into the k-means clustering model. First, the number of clusters is set to 5, the clustering center point is randomly determined, and the number of iterations is set to 25. Then, each grid cell with ten standardized terrain factors is classified into the corresponding cluster with the smallest distance to the final center point of the cluster through 25 iterative calculation. The five final center points of the clusters are shown in Table 4. Finally, all the grid cells are classified into five types of different terrain complexity levels, as shown in Figure 5b and Table 5.

Table 4. The final cluster center of normalized terrain factors.

Terrain Factor	1	2	3	4	5
elevation (*E*)	2.122	−0.489	−0.654	0.444	1.171
slope (*S*)	2.855	0.138	−0.801	0.190	1.462
plan curvature (*Plc*)	−0.706	−0.054	0.174	0.016	−0.391
profile curvature (*Prc*)	1.215	0.281	−0.681	0.305	1.095
relief amplitude (*Rel*)	2.752	0.240	−0.794	0.168	1.424
surface roughness (*Rou*)	2.765	0.146	−0.769	0.162	1.429
surface cutting depth (*Scd*)	3.940	−0.109	−0.548	−0.116	1.212
gully density (*Gd*)	0.407	1.745	−0.410	−0.251	0.284
elevation variation coefficient (*Evc*)	−0.372	0.322	0.259	−0.366	−0.301
slope length (*L*)	1.165	0.578	−0.979	0.749	0.959

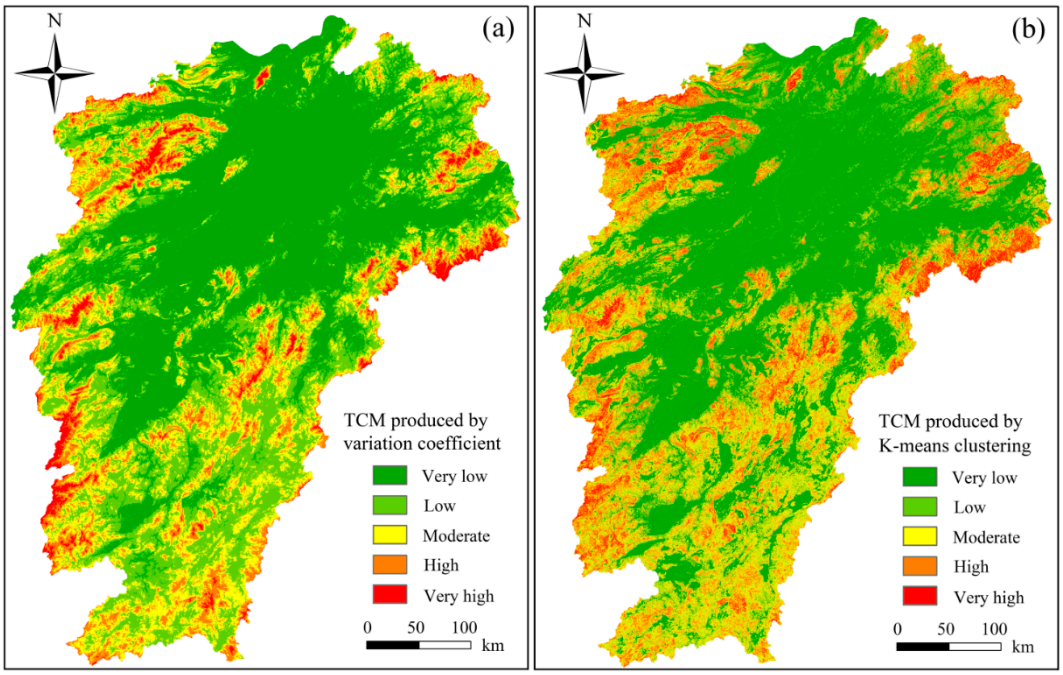

Figure 5. TCMs produced by variation coefficient method (**a**) and K-means clustering model (**b**).

Table 5. TCA results of the four models.

	PCA		Slope-Only		Variation Coefficient		K-Means Clustering	
TCA Level	**Area/km^2**	**Percentage/%**	**Area/km^2**	**Percentage/%**	**Area/km^2**	**Percentage/%**	**Area/km^2**	**Percentage/%**
very low	61,156	36.64	83,442	50.00	66,395	39.78	74,493	44.63
low	67,954	40.72	56,538	33.88	48,384	28.99	19,004	11.39
moderate	25,274	15.14	22,409	13.43	32,383	19.40	45,098	27.02
high	10,078	6.04	4271	2.56	15,495	9.28	23,247	13.93
Very high	2438	1.46	240	0.14	4243	2.54	5058	3.03

4. Discussion

4.1. Accuracy Assessment of the Four Models

In order to analyze the TCA accuracy of the PCA, slope-only, variable coefficient and k-means clustering models, the correlation coefficients between the TCMs produced by the four models and the local topographic map obtained from the government field surveys are calculated, respectively. A greater correlation coefficient value means that the produced TCM and the topographic map matches better, which further suggests higher TCA accuracy.

In this study, the topographic map with a scale of 1: 250,000, surveyed by the Bureau of Land and Resources of Jiangxi province in 2015, is used to evaluate the TCA accuracy of the four models. In the topographic map of Jiangxi province, the topographic types are classified as five categories of plain, hill, low mountain, middle mountain and mountain, which are assigned values of 1, 2, 3, 4, 5, respectively (Figure 6). In order to compare the TCMs with the topographic map, the produced TCMs are classified into five terrain complexity levels of very low, low, moderate, high and very high, which are also assigned values of 1, 2, 3, 4, 5, respectively. Then, the correlation coefficients between the topographic map and the TCMs produced by the PCA, slope-only, variable coefficient and K-means clustering models are calculated as 0.894, 0.763, 0.816 and 0.788, respectively. The results show that the TCM produced by the PCA method has the highest correlation coefficient with the topographic map compared to those produced by the slope-only, variable coefficient and k-means clustering models. That is to say, the PCA model has much higher TCA accuracy than the other three types of models.

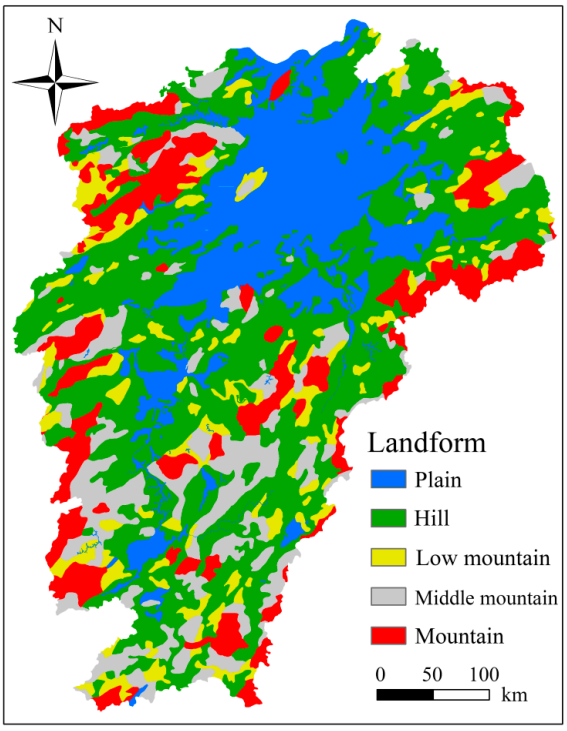

Figure 6. Landscape map with 1:250,000 scale in Jiangxi province.

4.2. TCA Compared with Three-Dimensional Aerial Images

In order to more intuitively reflect the consistency between the TCA performance and the actual terrain features, the TCM produced by the PCA method is compared with three-dimensional aerial images of the study area. Eight locations in the TCM are randomly selected, and the three-dimensional aerial images of these locations (Figure 7a–h) are acquired correspondingly. Taking Figure 7a–e as examples,

(1) The topographic complexity levels of Figure 7a,d are mainly high and very high, which is highly consistent with the three-dimensional aerial images of Figure 7a,d. Generally, the topography types of Figure 7a,d are dominated by mountains and valleys.

(2) The topographic complexity levels in both Figure 7b,c are low and the corresponding elevation variations are small. Meanwhile, the topographic features shown in the three-dimensional aerial images of Figure 7b,c are plain and hill. Hence, the matching degree between the TCA result and the three-dimensional aerial image is very high.

(3) A mixture of several kinds of topographic complexity levels is shown in Figure 7e, which is also very consistent with the topographic features of rolling hills and low mountains shown in the aerial image of Figure 7e. The above analysis shows that the TCA accuracy of the PCA method is high and the terrain complexity maps match well with the actual three-dimensional aerial images.

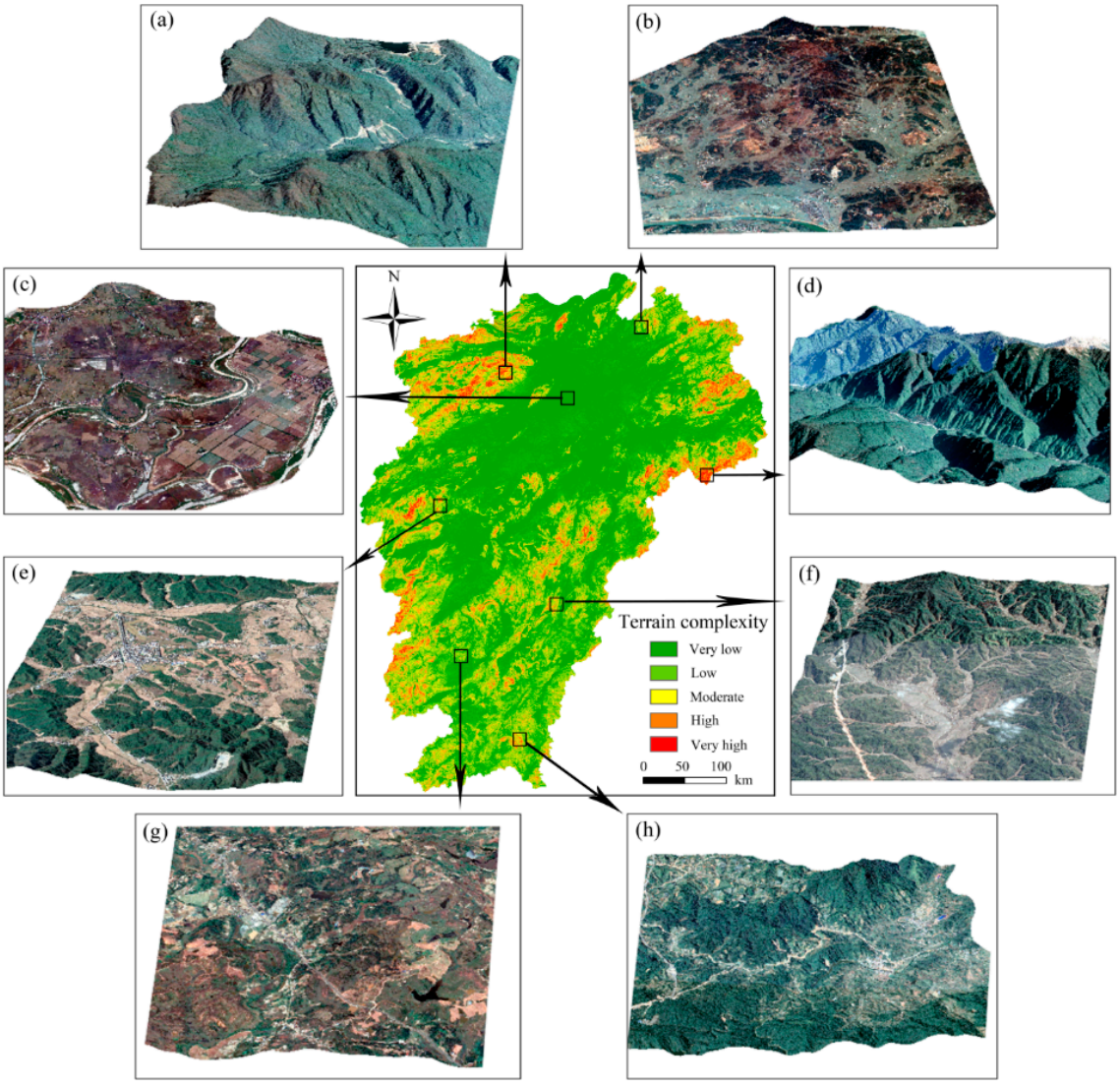

Figure 7. Topographic complexity map and its corresponding three-dimensional aerial images.

4.3. Limitations and Research Prospects

Although the PCA method used in this study shows better TCA performance than the other three types of methods, there are still some limitations in the processes of PCA modeling. Firstly, it is necessary to further test the accuracy of the original DEM data and strive to obtain DEM data with higher accuracy on this basis. Secondly, the DEM spatial resolution of 100 m is relatively rough; hence, DEM data with higher spatial resolution is needed in order to implement TCA modeling in further research. Thirdly, only ten kinds of terrain factors are extracted from the DEM data in this study; it is significant to extract more terrain factors from DEM data, such as ridge lines, valley lines, slope forms, etc. In the next study, more terrain factors will be introduced as the input variables of the PCA method. Fourthly, the main features extracted by the PCA are the linear correlations among all these terrain factors, and the subsequent research will extract more nonlinear features among the terrain factors. Therefore, kernel principal component analysis [62] or other nonlinear data compression methods can be considered in order to carry out this study. Finally, the accuracy of terrain complexity assessment should be analyzed and verified by combining it with field investigation in the next research, and the engineering applications of TCA results in various fields should be explored to enhance the research significance of this study.

In addition, for the use of the PCA method, all the data sets are put into the PCA method to calculate terrain complexity indexes. However, there is a lack of statistical validation of the results, as a result, an estimate of the goodness of the model itself is not present in this study. Hence, compared to the unsupervised models used in this study, some supervised mathematical models will be used to implement TCA in the next study. For the supervised mathematical models, some of the data sets are used to create a model and the remaining are used to give an estimate of the goodness of the model itself. Furthermore, it is necessary to make sure that the accuracy of the description of the territory using only the new variables is homogeneous over the whole territory. Hence, in the next study, we need to repeat the construction of the models many times using each time a subset of the available data (typically two or three of the datasets) extracted randomly.

5. Conclusions

There are some disadvantages in the previous TCA studies, such as few terrain factors used for TCA modeling, the lack of information compression between terrain factors and the qualitative TCA modeling processes. In order to overcome these disadvantages, a PCA method is introduced to carry out TCA in this study. The Jiangxi province of China with complex terrain features is used as the study area. Ten terrain factors including elevation, slope, plan curvature, profile curvature, relief amplitude, surface roughness, surface cutting depth, gully density, elevation variation coefficient and slope length are selected as input variables of PCA. The TCM produced by PCA is compared with the results of slope-only, variation coefficient and K-means clustering models and is also verified by aerial images obtained by field survey.

It can be concluded that the PCA method can accurately and reliably describe the terrain complexity distribution features; the produced TCM is very consistent with the actual terrain features. In addition, the proposed PCA method has considerably higher accuracy than the other three models. The main contributions of this study include the comprehensive consideration of ten related terrain factors to address TCA, the removal of redundant information in these terrain factors and the quantitative calculation of terrain complexity indexes. Hence, the TCM produced in this study can be applied to improve the local geological investigation and land planning utilization.

Author Contributions: Conceptualization: Faming Huang, Yijing Li and Jianbo Yang; methodology: Faming Huang and Jianbo Yang; software: Jianbo Yang; validation: Jinsong Huang, and Biao Zhang; formal analysis: Na Chen; investigation: Jianbo Yang; resources: Faming Huang; data curation: Yijing Li; writing—original draft preparation: Faming Huang, Jianbo Yang, and Yijing Li; writing—review and editing: Faming Huang and Jinsong Huang; visualization: Biao Zhang; supervision: Yijing Li; project administration: Faming Huang;

funding acquisition: Faming Huang and Yijing Li. All authors have read and agreed to the published version of the manuscript.

Funding: This study was supported by the National Natural Science Foundation of China (NOs. 41807285, 41972280, 40501454 and 41501454), National Science Foundation of Jiangxi Province of China (NO. 20192BAB216034), the Postdoctoral Science Foundation of Jiangxi Province of China (NO. 2019KY08), the China Postdoctoral Science Foundation (NOs. 2019M652287 and 2020T130274) and Science and Technology Project of Water Resources Department of Jiangxi Province (NO. KT201544).

Acknowledgments: This study was supported by the National Natural Science Foundation of China (NOs. 41807285, 41972280, 40501454 and 41501454), National Science Foundation of Jiangxi Province of China (NO. 20192BAB216034), the Postdoctoral Science Foundation of Jiangxi Province of China (NO. 2019KY08), the China Postdoctoral Science Foundation (NOs. 2019M652287 and 2020T130274) and Science and Technology Project of Water Resources Department of Jiangxi Province (NO. KT201544).

Conflicts of Interest: The authors declare no conflict of interest.

References

1. Huang, C.; Yang, J.; Jiang, P. Assessing impacts of urban form on landscape structure of urban green spaces in china using landsat images based on google earth engine. *Remote Sens.* **2018**, *10*, 1569. [CrossRef]
2. Levin, E.; Shults, R.; Habibi, R.; An, Z.; Roland, W. Geospatial virtual reality for cyberlearning in the field of topographic surveying: Moving towards a cost-effective mobile solution. *ISPRS Int. J. Geo-Inf.* **2020**, *9*, 433. [CrossRef]
3. Li, S.; Zhang, S.; Li, T.; Gao, Y.; Chen, Q.; Zhang, X. Modeling the optimal baseline for a spaceborne bistatic sar system to generate dems. *ISPRS Int. J. Geo-Inf.* **2020**, *9*, 108. [CrossRef]
4. Jaljolie, R.; Van Oosterom, P.; Dalyot, S. Spatial data structure and functionalities for 3d land management system implementation: Israel case study. *ISPRS Int. J. Geo-Inf.* **2018**, *7*, 10. [CrossRef]
5. Ha, T.; Choi, J.Y.; Yoo, J.; Chun, I.; Shim, J. Transformation of small-scale meteorological tsunami due to terrain complexity on the western coast of korea. *J. Coast. Res.* **2014**, *70*, 284–289. [CrossRef]
6. Farmakis-Serebryakova, M.; Hurni, L. Comparison of relief shading techniques applied to landforms. *ISPRS Int. J. Geo-Inf.* **2020**, *9*, 253. [CrossRef]
7. Yang, X.; Tang, G.; Meng, X.; Xiong, L. Saddle position-based method for extraction of depressions in fengcong areas by using digital elevation models. *ISPRS Int. J. Geo-Inf.* **2018**, *7*, 136. [CrossRef]
8. Aguilar, F.J.; Agüera, F.; Aguilar, M.A.; Carvajal, F. Effects of terrain morphology, sampling density, and interpolation methods on grid dem accuracy. *Photogramm. Eng. Remote Sens.* **2005**, *71*, 805–816. [CrossRef]
9. Liu, Y.B.; Smedt, F.D.; Hoffmann, L.; Pfister, L. Assessing land use impacts on flood processes in complex terrain by using gis and modeling approach. *Environ. Model. Assess.* **2005**, *9*, 227–235. [CrossRef]
10. Huang, F.; Chen, L.; Yin, K.; Huang, J.; Gui, L. Object-oriented change detection and damage assessment using high-resolution remote sensing images, tangjiao landslide, three gorges reservoir, china. *Environ. Earth Sci.* **2018**, *77*, 183. [CrossRef]
11. Prasannakumar, V.; Vijith, H.; Geetha, N. Terrain evaluation through the assessment of geomorphometric parameters using DEM and GIS: Case study of two major sub-watersheds in Attapady, South India. *Arab. J. Geosci.* **2013**, *6*, 1141–1151. [CrossRef]
12. Tianwen, L.I.; Liu, X.; Tang, G. Influence of terrain complexity on slope and aspect. *J. Mt. Res.* **2004**, *22*, 272–277.
13. Huaxing, L.U.; Liu, X.; Tang, G. Terrain complexity assessment based on multivariate analysis. *J. Mt. Sci.* **2012**, *30*, 616–621.
14. Long, Y.; Zhou, T.; Tang, G.; Liu, X. Research on terrain complexity of several typical regions of loess landform based on fractal method. *J. Mt. Sci.* **2007**, *25*, 385–392.
15. Ashenfelter, K.T.; Eberhard, K.M. Effects of verb complexity on speech errors. *Mem. Cogn.* **2007**, *35*, 1527–1541. [CrossRef]
16. Chambers, T.C.; Drinnan, A.N.; Mcloughlin, S. Some morphological features of wollemi pine (wollemia nobilis: Araucariaceae) and their comparison to cretaceous plant fossils. *Int. J. Plant. Sci.* **1998**, *159*, 160–171. [CrossRef]
17. Rawat, J.S.; Joshi, R.C. Remote-sensing and gis-based landslide-susceptibility zonation using the landslide index method in igo river basin, eastern himalaya, india. *Int. J. Remote Sens.* **2012**, *33*, 3751–3767. [CrossRef]

18. Thompson, J.A.; Bell, J.C.; Butler, C.A. Digital elevation model resolution: Effects on terrain attribute calculation and quantitative soil-landscape modeling. *Geoderma* **2015**, *100*, 67–89. [CrossRef]
19. Bartlett, M.S.; Movellan, J.R.; Sejnowski, T.J. Face recognition by independent component analysis. *IEEE Trans. Neural Netw.* **2002**, *13*, 1450–1464. [CrossRef]
20. Gasmi, A.; Gomez, C.; Zouari, H.; Masse, A.; Ducrot, D. Pca and svm as geo-computational methods for geological mapping in the southern of tunisia, using aster remote sensing data set. *Arab. J. Geosci.* **2016**, *9*, 753. [CrossRef]
21. Lan, L.; Li, C.F.; Lei, Y.M.; Yin, J.Y.; Zhao, J.J. Feature extraction for hyperspectral remote sensing image using weighted pca-ica. *Arab. J. Geosci.* **2017**, *10*, 307.
22. Zhao, X.; Wang, W.; Chu, X.; Li, C.; Kimuli, D. Early detection of aspergillus parasiticus infection in maize kernels using near-infrared hyperspectral imaging and multivariate data analysis. *Appl. Sci.* **2017**, *7*, 90. [CrossRef]
23. Marchetti, M.; Offroy, M.; Abdat, F.; Branchu, P.; Bourson, P.; Jobard, C.; Durmont, J.-F.; Casteran, G. Chemometrics-assisted monitoring in raman spectroscopy for the biodegradation process of an aqueous polyfluoroalkyl ether from a fire-fighting foam in an environmental matrix. *Environments* **2020**, *7*, 4. [CrossRef]
24. Li, H.; Zhang, Z.; Yin, X. A novel probabilistic power flow algorithm based on principal component analysis and high-dimensional model representation techniques. *Energies* **2020**, *13*, 3520. [CrossRef]
25. Geng, D.; Zhang, H.; Wu, H. Short-term wind speed prediction based on principal component analysis and lstm. *Appl. Sci.* **2020**, *10*, 4416. [CrossRef]
26. Schwartz, C.; Ramos, L.P.; Duarte, L.T.; Pinho, M.d.S.; Pettersson, M.I.; Vu, V.T.; Machado, R. Change detection in uwb sar images based on robust principal component analysis. *Remote Sens.* **2020**, *12*, 1916. [CrossRef]
27. Gao, J.; Chai, S.; Zhang, B.; Xia, Y. Research on network intrusion detection based on incremental extreme learning machine and adaptive principal component analysis. *Energies* **2019**, *12*, 1223. [CrossRef]
28. Samsonov, T.E. Automated conflation of digital elevation model with reference hydrographic lines. *ISPRS Int. J. Geo-Inf.* **2020**, *9*, 334. [CrossRef]
29. Huang, F.; Cao, Z.; Jiang, S.-H.; Zhou, C.; Huang, J.; Guo, Z. Landslide susceptibility prediction based on a semi-supervised multiple-layer perceptron model. *Landslides* **2020**. [CrossRef]
30. Pham, B.T.; Bui, D.T.; Prakash, I.; Dholakia, M.B. Hybrid integration of multilayer perceptron neural networks and machine learning ensembles for landslide susceptibility assessment at himalayan area (india) using gis. *Catena* **2017**, *149*, 52–63. [CrossRef]
31. Huang, F.; Yin, K.; Huang, J.; Lei, G.; Peng, W. Landslide susceptibility mapping based on self-organizing-map network and extreme learning machine. *Eng. Geol.* **2017**, *223*, 11–22. [CrossRef]
32. Zhu, L.; Huang, L.; Fan, L.; Huang, J.; Huang, F.; Chen, J.; Zhang, Z.; Wang, Y. Landslide susceptibility prediction modeling based on remote sensing and a novel deep learning algorithm of a cascade-parallel recurrent neural network. *Sensors* **2020**, *20*, 1576. [CrossRef] [PubMed]
33. Li, D.; Huang, F.; Yan, L.; Cao, Z.; Chen, J.; Ye, Z. Landslide susceptibility prediction using particle-swarm- optimized multilayer perceptron: Comparisons with multilayer-perceptron-only, bp neural network, and information value models. *Appl. Sci.* **2019**, *9*, 3664. [CrossRef]
34. Chang, Z.; Du, Z.; Zhang, F.; Huang, F.; Chen, J.; Li, W.; Guo, Z. Landslide susceptibility prediction based on remote sensing images and gis: Comparisons of supervised and unsupervised machine learning models. *Remote Sens.* **2020**, *12*, 502. [CrossRef]
35. Huang, F.; Cao, Z.; Guo, J.; Jiang, S.-H.; Li, S.; Guo, Z. Comparisons of heuristic, general statistical and machine learning models for landslide susceptibility prediction and mapping. *CATENA* **2020**, *191*, 104580. [CrossRef]
36. Huang, F.; Chen, J.; Du, Z.; Yao, C.; Huang, J.; Jiang, Q.; Chang, Z.; Li, S. Landslide susceptibility prediction considering regional soil erosion based on machine-learning models. *ISPRS Int. J. Geo-Inf.* **2020**, *9*, 377. [CrossRef]
37. Hong, H.; Ilia, I.; Tsangaratos, P.; Chen, W.; Xu, C. A hybrid fuzzy weight of evidence method in landslide susceptibility analysis on the wuyuan area, china. *Geomorphology* **2017**, *290*, 1–16. [CrossRef]
38. Huang, F.; Yao, C.; Liu, W.; Li, Y.; Liu, X. Landslide susceptibility assessment in the nantian area of china: A comparison of frequency ratio model and support vector machine. *Geomat. Nat. Hazards Risk* **2018**, *9*, 919–938. [CrossRef]

39. Han, X.Y.; Qian, J.; Wang, L.; Liu, F.; Mao, Z.Q. Progress in studying multi-scale process of soil erosion(water erosion) and soil conservation in the loess plateau. *J. Glaciol. Geocryol.* **2012**, *34*, 1487–1498.
40. Liu, W.; Wan, S.; Huang, F.; Luo, X.; Fu, M. Experimental study of subsurface erosion in granitic under the conditions of different soil column angles and flow discharges. *Bull. Eng. Geol. Environ.* **2019**, *78*, 5877–5888. [CrossRef]
41. Li, Y.; Huang, J.; Jiang, S.-H.; Huang, F.; Chang, Z. A web-based gps system for displacement monitoring and failure mechanism analysis of reservoir landslide. *Sci. Rep.* **2017**, *7*, 17171. [CrossRef]
42. Huang, F.; Yin, K.; Zhang, G.; Zhou, C.; Zhang, J. Landslide groundwater level time series prediction based on phase space reconstruction and wavelet analysis-support vector machine optimized by pso algorithm. *Earth Sci. J. China Univ. Geosci.* **2015**, *40*, 1254–1265.
43. Huang, F.; Zhang, J.; Zhou, C.; Wang, Y.; Huang, J.; Zhu, L. A deep learning algorithm using a fully connected sparse autoencoder neural network for landslide susceptibility prediction. *Landslides* **2020**, *17*, 217–229. [CrossRef]
44. Lin, G.F.; Chang, M.J.; Huang, Y.C.; Ho, J.Y. Assessment of susceptibility to rainfall-induced landslides using improved self-organizing linear output map, support vector machine, and logistic regression. *Eng. Geol.* **2017**, *224*, 62–74. [CrossRef]
45. Szymura, T.H.; Szymura, M.; Pietrzak, M. Influence of land relief and soil properties on stand structure of overgrown oak forests of coppice origin with sorbus torminalis. *Dendrobiology* **2014**, *71*, 49–58. [CrossRef]
46. Liu, L. The ups and downs of North America: Evaluating the role of mantle dynamic topography since the mesozoic. *Rev. Geophys.* **2015**, *53*, 1022–1049. [CrossRef]
47. Zhang, F.; Chen, L.I.; Meng, B.; Zhao, H.; Liu, Z. Investigation of surface deformation characteristic and removal mechanism for k9 glass based on varied cutting-depth nano-scratch. *J. Mech. Eng.* **2016**, *52*, 65–71. [CrossRef]
48. Parhad, P.; Likhite, A.; Bhatt, J.; Peshwe, D. The effect of cutting speed and depth of cut on surface roughness during machining of austempered ductile iron. *Trans. Indian Inst. Met.* **2015**, *68*, 99–108. [CrossRef]
49. Robinson, I.K. Crystal truncation rods and surface roughness. *Phys. Rev. B Condens. Matter* **1986**, *33*, 3830. [CrossRef]
50. Zhao, J.; Vanmaercke, M.; Chen, L.; Govers, G. Vegetation cover and topography rather than human disturbance control gully density and sediment production on the chinese loess plateau. *Geomorphology* **2016**, *274*, 92–105. [CrossRef]
51. Guo, Z.; Yin, K.; Gui, L.; Liu, Q.; Huang, F.; Wang, T. Regional rainfall warning system for landslides with creep deformation in three gorges using a statistical black box model. *Sci. Rep.* **2019**, *9*, 8962. [CrossRef]
52. Kaneta, M.; Miyai, N.; Yamamoto, M.; Oka, M.; Utsumi, M.; Shiba, M.; Arita, M. 3d.08: Arterial stiffness and autonomic nervous function on orthostatic blood pressure-elevation in hypertensive patients. *J. Hypertens.* **2015**, *33* (Suppl. 1), e42. [CrossRef]
53. Tubaro, M.; Sciahbasi, A.; Ricci, R.; Ciavolella, M.; Di, C.D.; Bisconti, C.; Ferraiuolo, G.; Del, P.M.; Mennuni, M.; Monti, F. Early invasive versus early conservative strategy in non-st-elevation acute coronary syndrome: An outcome research study. *Eur. Heart J. Acute Cardiovasc. Care* **2017**, *76*, 511–527. [CrossRef] [PubMed]
54. Liu, B.Y.; Nearing, M.A.; Shi, P.J.; Jia, Z.W. Slope length effects on soil loss for steep slopes. *Soil Sci. Soc. Am. J.* **2000**, *64*, 1759–1763. [CrossRef]
55. Huang, F.; Chen, J.; Yao, C.; Chang, Z.; Jiang, Q.; Li, S.; Guo, Z. Susle: A slope and seasonal rainfall-based rusle model for regional quantitative prediction of soil erosion. *Bull. Eng. Geol. Environ.* **2020**. [CrossRef]
56. Malhi, A.; Gao, R.X. Pca-based feature selection scheme for machine defect classification. *IEEE Trans. Instrum. Meas.* **2004**, *53*, 1517–1525. [CrossRef]
57. Eldridge, S.M.; Ashby, D.; Kerry, S. Sample size for cluster randomized trials: Effect of coefficient of variation of cluster size and analysis method. *Int. J. Epidemiol.* **2006**, *35*, 1292. [CrossRef] [PubMed]
58. Weiss, E.; Milich, L. Errors in a standard method for generating interannual ndvi coefficient of variation (cov) images. *Int. J. Remote Sens.* **1997**, *18*, 3743–3748. [CrossRef]
59. Çoşkun, G. A new slip safety risk scale of natural stones with statistical k-means clustering analysis. *Arab. J. Geosci.* **2018**, *11*, 799. [CrossRef]
60. Moghimi, A.; Khazai, S.; Mohammadzadeh, A. An improved fast level set method initialized with a combination of k-means clustering and otsu thresholding for unsupervised change detection from sar images. *Arab. J. Geosci.* **2017**, *10*, 293. [CrossRef]

61. Tipping, M.E.; Bishop, C.M. Mixtures of probabilistic principal component analyzers. *Neural Comput.* **2014**, *11*, 443–482. [CrossRef]
62. Zhao, Y.N.; Niu, R.Q.; Li, J.; Peng, L.; Wang, Y. Prediction of landslide displacement based on kernel principal component analysis and neural network-markov chain. In *Advanced Materials Research*; Trans Tech Publ.: Freienbach, Switzerland, 2013; pp. 1512–1520.